

Broadband Diffractive Solar Sail

PRATEEK R. SRIVASTAVA,¹ RYAN M. CRUM,¹ AND GROVER A. SWARTZLANDER, JR.^{1,*}

¹*Chester F. Carlson Center for Imaging Science, Rochester Institute of Technology, Rochester, NY 14623, USA*

**grover.swartzlander@gmail.com*

Abstract: The transverse radiation pressure force and acceleration is compared for two parametrically optimized designs: prismatic and two-pillar metasurface gratings. The numerical results were cross-verified with both Maxwell stress tensor and modal analysis. Solar blackbody irradiance was assumed for wavelengths ranging from $0.33 \mu\text{m}$ to the grating cutoff at $1.5 \mu\text{m}$, encompassing 83% of the solar constant. This multi-objective optimizer study found that neither design comprised of Si_3N_4 performed as well as those corresponding to a low refractive index, low mass density material. The predicted transverse acceleration of the optimized low-index metasurface grating is compared to that of a state-of-the-art reflective solar sail.

1. Introduction

The in-space propulsion of sailcraft via solar radiation pressure was originally pioneered by in the 1920s by Tsander and Tsiolkvosy [1,2]. In contrast to rockets which both transport significant amounts of fuel mass and make discrete orbit-changing burns, solar sails can attain extraordinarily high velocities given a low mass and continuous acceleration. Space organizations such as NASA, JAXA, and the Planetary Society, have improved the technical readiness level of solar sails in recent years, culminating in an assortment of proposed space science missions [3]. The advent of solar sailing has stimulated advanced concepts that consider the mission objectives as part of the sail design. For example, missions having a spiral trajectory toward or away from the sun benefit from a sail having an optimal “lift” force perpendicular to the sun line. To achieve lift a traditional reflective sail must be tilted away from the sun; consequently the maximum lift cannot be achieved owing to the reduced illumination projected area. In contrast, optical scattering mechanisms like diffraction provide alternative means of transferring photon momentum to the sail in a preferred sun-facing orientation [4–16]. The maximum transverse force on the sail occurs when sunlight is uniformly scattered at 90° with respect to the surface normal of a sun-facing sail.

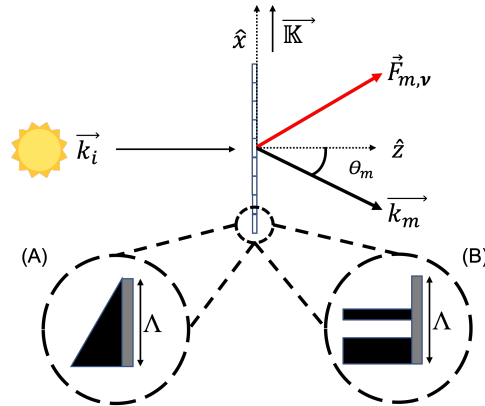


Fig. 1. Schematic diagram of a solar sail with constituent (A) prism and (B) subwavelength pillar elements of period Λ and. The sail diffracts incident light \vec{k}_i by θ_m into \vec{k}_m owing to \vec{K} , resulting in net radiation pressure force \vec{F} .

2. Theory

To advance the understanding of diffractive sails we explore two designs: a triangular prismatic grating and a metasurface grating comprised of two pillars. Two material strategies are analyzed for each design. First we consider an arbitrary non-dispersive dielectric material having a refractive index n_1 placed on a thin substrate of index $n_2 = 1.5$. Finite difference time domain (FDTD) methods are used to account for internal and external reflections of both polarization component of light, and moreover, the angular scattering distribution across a broad band of optical frequencies. Likewise, we determine the angular scattering distribution when the grating and thin substrate are made with Si_3N_4 . The schematic illustration shown in Fig. 1 depicts a portion of a flat rigid infinitely periodic grating with period Λ in the x, z -plane of incidence for a sun-facing configuration, comprised of either (A) prism elements or (B) pillars on a thin substrate. Structural flexing and non-normal incidence angle are beyond the scope of this baseline study. The grating period $\Lambda = 1.5$ [μm], or equivalently the grating frequency $\tilde{\nu} = c/\Lambda = 200$ [THz] was selected from a consideration of the spectral cut-off condition, the prism mass, and diffraction effects. The fraction of blackbody irradiance cut off from diffraction decreases with increasing value of Λ , whereas the mass of a prism varies as Λ^2 . A large value of the transverse acceleration generally requires negligible spectral cut off and low mass, which combined with a diffraction analysis, provides a value of roughly $\Lambda = 1.5$ [μm].

Light is transmitted or reflected light into discrete diffraction angles θ_m measured with respect to the back surface normal as depicted in Fig. 1. In the reference frame of the sail, the incident and scattered wavelengths are equal, and thus, the respective wave vectors may be expressed $\vec{k}_i = k\hat{z}$ and $\vec{k}_m = k(\cos\theta_m\hat{z} + \sin\theta_m\hat{x})$, where $k = 2\pi/\lambda$. The diffraction angles are governed by the grating equation: $\sin\theta_m = m\lambda/\Lambda$ assuming normal incidence. We note that $\cos\theta_m = \pm\sqrt{1 - \sin^2\theta_m}$, where $+$ ($-$) corresponds to transmitted (reflected) light. The m^{th} order photon momentum transfer efficiency imparted to the sail at the optical frequency $\nu = c/\lambda$ may be expressed $\vec{\eta}_{\nu,m} = (\vec{k}_i - \vec{k}_m)/k = (1 - \cos\theta_m)\hat{z} - \sin\theta_m\hat{x}$, where c is the speed of light, and normal incidence is assumed. For a light source having a spectral irradiance distribution $\tilde{I}(\nu)$ the net momentum transfer efficiency $\vec{\eta}$ may be found by integrating over all frequencies and summing over all allowed diffraction orders for both polarization modes [12]. For an unpolarized source like the sun, we assume the spectral irradiance is equally divided into s and p polarization states.

The net radiation pressure force on the sail may be expressed $\vec{F} = F_0\vec{\eta}$, where $F_0 = I_0A/c$ where A is the sail area and I_0 is the irradiance. For example the solar blackbody irradiance between ν_{\min} and ν_{\max} of a band-limited blackbody source a distance r from the sun may be expressed

$$I_0 = \frac{R_S^2}{r^2} \int_{\nu_{\min}}^{\nu_{\max}} \tilde{I}(\nu) d\nu = \frac{R_S^2}{r^2} \frac{2\pi h}{c^2} \int_{\nu_{\min}}^{\nu_{\max}} \frac{\nu^3 d\nu}{\exp(h\nu/k_B T) - 1} \quad (1)$$

where $R_S = 6.957 \times 10^8$ [m] is the solar radius, $h = 6.626 \times 10^{-34}$ [J · s] is the Planck constant, $k_B = 1.381 \times 10^{-23}$ [J/K] is the Boltzmann constant, and we assign $T = 5770.2$ as the effective absolute temperature of the sun. Below we assume r corresponds to 1 [AU]. The case $\nu_{\min, \max} = 0, \infty$ corresponds to the so-called solar-constant, $I_{\text{sun}} = 1360$ [W/m²]. Values of I_0 are plotted in Fig. 2 as a function of the grating period for $\nu_{\min} = \tilde{\nu} = c/\Lambda$ and two different values of ν_{\max} : ∞ (blue line) and 900 [THz] (red line). The case used for our FDTD model, $\lambda_{\min} = 0.333$ [μm] and $\lambda_{\max} = \Lambda = 1.5$ [μm] ($\nu_{\min} = 200$ [THz], and $\nu_{\max} = 900$ [THz]) includes up to four diffraction orders and spans 83% of the solar spectrum. Although wider bandwidths are of interest, FDTD run times become prohibitively long.

Following Ref [12] the net radiation pressure force on the sail owing to a band-limited source

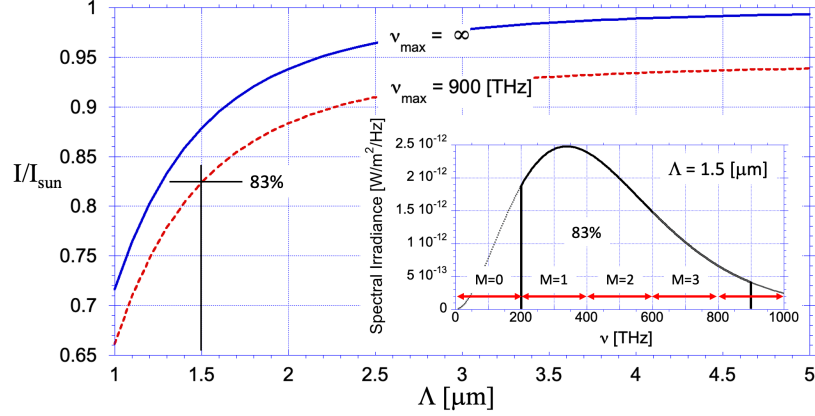


Fig. 2. Fraction of integrated solar black body spectral irradiance for the range $\nu_{min} = c/\Lambda$ to ν_{max} , where $I_{sun} = 1360$ [W/m^2]. Insert: Black body spectral irradiance with range $\nu_{min} = 200$ [THz] ($\Lambda = 1.5$ [μm]) and $\nu_{max} = 900$ [THz] ($0.83I_{sun}$). Arrows: Range of maximum mode number M .

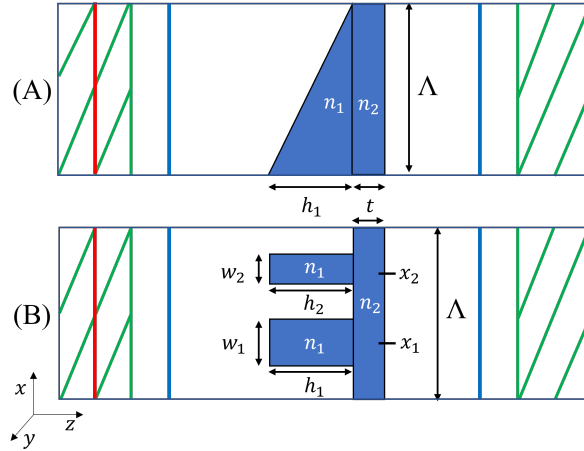


Fig. 3. FDTD Schematic: Unit cell of period Λ of (A) prism and (B) meta gratings with plane wave source (red line), field monitors (blue lines), and perfectly absorbing boundary layers (green areas).

may be expressed

$$\vec{F}^{s,p} = \frac{A}{c} \int_{\nu_{min}}^{\nu_{max}} \sum_{m=M_{\nu}^{-}}^{M_{\nu}^{+}} \tilde{I}_m^{s,p}(\nu) ((1 - \cos \theta_m) \hat{z} - \sin \theta_m \hat{x}) d\nu \quad (2)$$

where $\tilde{I}_m^s(\nu)$ and $\tilde{I}_m^p(\nu)$ respectively correspond to the value of the spectral irradiance scattered into the m^{th} diffraction order for the s and p polarization states, and where θ_m depends on frequency owing to the grating equation which may be expressed, $\sin \theta_m = mc/\nu\Lambda$. The frequency-dependent cut-off mode numbers at the normal incident are given by $M_{\nu}^{\pm} = \pm \text{INT}[\nu/\tilde{\nu}]$ (or equivalently $\pm \text{INT}[\Lambda/\lambda]$) where INT represents the integer value of the argument rounded toward zero. In a lossless system having no guided surface waves that extend to infinity, we

expect

$$\tilde{I}(\nu) = \sum_{m=M_{\bar{\nu}}^-}^{M_{\bar{\nu}}^+} (\tilde{I}_m^s(\nu) + \tilde{I}_m^p(\nu)) \quad (3)$$

In general $\tilde{I}_m^s(\nu) \neq \tilde{I}_m^p(\nu)$ owing to polarization-dependent scattering.

The Maxwell stress tensor $\overline{\overline{T}}_{\nu}$ may be evaluated at each frequency as an alternative method to evaluate the net force \vec{F} :

$$\vec{F}^{s,p} = \int_{\nu_{\min}}^{\nu_{\max}} \vec{F}_{\nu}^{s,p} d\nu = \int_{\nu_{\min}}^{\nu_{\max}} \left(\oint_S \overline{\overline{T}}_{\nu,ij}^{s,p} \cdot d\vec{S} \right) d\nu \quad (4)$$

where S is an arbitrary surface enclosing the sail, $d\vec{S}$ is the elemental area vector and

$$\overline{\overline{T}}_{\nu,ij}^{s,p} = \epsilon_0 (E_{\nu,i}^{s,p} E_{\nu,j}^{s,p} - \frac{1}{2} |E_{\nu}^{s,p}|^2 \delta_{ij}) + \frac{1}{\mu_0} (B_{\nu,i}^{s,p} B_{\nu,j}^{s,p} - \frac{1}{2} |B_{\nu}^{s,p}|^2 \delta_{ij}) \quad (5)$$

where ϵ_0 and μ_0 are respectively the vacuum permittivity and permeability, E and B are respectively electric and magnetic field amplitudes, and δ_{ij} is the Kronecker delta function. For a structure that is periodic in the plane of incidence as depicted in Fig. 3 and extended over a distance L_y out of the plane, the only elemental areas that contribute to (4) are $d\vec{S}_{z=\pm z_0} = \pm dx dy \hat{x} \pm dx dy \hat{z}$. The force exerted across the area $L_y \times \Lambda$ of an infinitely period grating may therefore be expressed

$$\begin{aligned} \vec{F}^{s,p} &= \int_{\nu_{\min}}^{\nu_{\max}} \left(\int_{\Lambda L_y} \left((\overline{\overline{T}}_{\nu,ij}^{s,p} \cdot d\vec{S})_{z=-z_0} + (\overline{\overline{T}}_{\nu,ij}^{s,p} \cdot d\vec{S})_{z=+z_0} \right) \right) d\nu \\ &= L_y \int_0^{\Lambda} \left((-T_{xx} - T_{zz})_{z=-z_0} + (T_{xx} + T_{zz})_{z=+z_0} \right) dx \end{aligned} \quad (6)$$

where z_0 is an arbitrary distance from the grating, and the final integral includes the frequency-integrated stress tensor components T_{xx} and T_{zz} .

3. Numerical Methods

We used the open source FDTD numerical solver MEEP [17] to solve Eq.s (4) - (6), making use of fast built-in "methods" like `ForceSpectra` to calculate forces in a specified `ForceRegion`. To cross-validate the force values we randomly compared them to values obtained using Eq.(2), this time using diffraction mode options in MEEP. In both cases, Bloch periodic boundary conditions were employed. The power spectrum of a broadband source in MEEP is defined as the distribution function `GaussianSource(fcen, fwidth)` where `fcen` and `fwidth` are respectively the center and width of the Gaussian distribution. Force calculations are made in the frequency domain and we scaled them to correspond to the solar blackbody spectral irradiance. The red line in Fig. 3 depicts a planar light source propagating in the \hat{z} direction. The blue lines represent so-called monitors where the electromagnetic fields $\vec{E}_{\nu}^{s,p}$ and $\vec{B}_{\nu}^{s,p}$ are evaluated for the determination of the Maxwell stress tensor, and where alternatively the spectral irradiance $\tilde{I}_m^{s,p}(\nu)$ may be determined to evaluate Eq. (2). The green lines in Fig. 3 represent perfectly matched layers. The square numerical grid elements were set to $\delta x = \delta z = 20$ [nm]. The simulation ran until either E_z or H_z decayed to 10^{-6} of the peak value.

The focus of this study was to determine optimized parameters of the two structures depicted in Fig. 3, both having the same period $\Lambda = 1.5$ [μm]: (A) a prismatic grating and substrate having four optimization parameters n_1, n_2, h_1 , and t ; and (B) a metasurface comprised of two pillars and a substrate having nine optimization parameters $n_1, n_2, h_1, h_2, w_1, w_2, x_1, x_2$, and t . We employed a multi-objective optimizer NSGA-II (with 40 agents, 40 offspring, 150

generations) [18] with the range of parameter values listed in Table 1. The objectives are to achieve the largest values of transverse force for both polarizations and to minimize the mass. A representative set of 40 solutions (called Pareto-optimal) were obtained. The same procedure was followed for silicon nitride ($n_{\text{Si}_3\text{N}_4}$) structures, but in this case $n_1 = n_2$ and $h_1 = h_2$. Silicon nitride is relatively stable in a space environment, its optical properties are well characterized, and its lithographic fabrication techniques are mature. The refractive index $n_{\text{Si}_3\text{N}_4}$ varies from ~ 2.00 at 200 [THz] to ~ 2.15 at 900 [THz] [19]:

$$n_{\text{Si}_3\text{N}_4}^2 - 1 = \frac{3.0249\lambda^2}{\lambda^2 - 0.1353406^2} + \frac{40314\lambda^2}{\lambda^2 - 1239.842^2} \quad (7)$$

A solar sail is typically used to achieve a spiral trajectory toward or away from the sun. In this case, the flight time may be minimized when the transverse (lift) component of acceleration F_x/M_{sc} is a maximum, where $M_{\text{sc}} = m_{\text{sail}} + m_{\text{pl}}$ is the total mass of the sailcraft, m_{sail} is the mass of the diffractive sail material, m_{pl} is the mass of the payload and structural support mechanisms, and $F_x = F_x^s + F_x^p$. The transverse acceleration is optimized when both F_x^s and F_x^p are maximized and m_{sail} is minimized. The sail mass of our two designs may be expressed

$$m_{\text{sail}}^{\text{prism}} = \left(\frac{1}{2}\rho_1 h + \rho_2 t\right) N_x^2 \Lambda^2 = \left(\frac{1}{2}\rho_1 h + \rho_2 t\right) A \quad (8a)$$

$$\begin{aligned} m_{\text{sail}}^{\text{meta}} &= \rho_1 (N_x w_1 h_1 + N_x w_2 h_2) N_x \Lambda + \rho_2 N_x^2 \Lambda^2 t \\ &= (\rho_1 w_1 h_1 / \Lambda + \rho_1 w_2 h_2 / \Lambda + \rho_2 t) A \end{aligned} \quad (8b)$$

where N_x is the number of grating periods across the sail, and A is the area of a square sail. Ignoring the payload mass ($m_{\text{pl}} = 0$) and writing the transverse component of force $F_x = I_0 A \eta_x / c = m_{\text{sail}} a_x$ we obtain the transverse acceleration for our unladen structures:

$$a_x^{\text{prism}} = \frac{I_0}{\alpha c} \frac{\eta_x}{\frac{1}{2}n_1 h + n_2 t} \quad (9a)$$

$$a_x^{\text{meta}} = \frac{I_0}{\alpha c} \frac{\eta_x}{n_1 (w_1 f_1 + w_2 f_2) + n_2 t} \quad (9b)$$

where $f_{1,2} = h_{1,2} / \Lambda$ is the fill factor, and for convenience we associate the refractive index and mass density with a proportionality factor α : $\rho_{1,2} \equiv \alpha n_{1,2}$. Using the space qualified polyimide material CP1 [20] as an example, with a specific gravity s.g. = 1.54 and a mean refractive index of 1.57 we obtain $\alpha = 0.98 \times 10^3$ [kg/m³]. For our silicon nitride structures we instead combine its specific gravity, s.g. = 3.17 [21] with the mean index, 2.02, to obtain $\alpha = 1.57 \times 10^3$ [kg/m³]. As seen in Eq. 9 the transverse acceleration is independent of the sail area and is implicitly dependent on the grating period Λ via the efficiency factor η_x (which is found by numerically determining the transverse force F_x value).

Table 1. Multi-Objective Optimization Scheme: Nine variables, three objectives, and four constraints.

| | |
|--------------------|---|
| x ∈ | $[x_{1,2}, w_{1,2}, h_{1,2}, n_{1,2}, t]$ |
| max : | $F_x^s(\mathbf{x}), F_x^p(\mathbf{x})$ |
| min : | mass(\mathbf{x}) |
| such that : | $1.5 \leq n_{1,2} \leq 3.5$ |
| such that : | $-\Lambda/2 \leq x_{1,2} \leq \Lambda/2$ |
| such that : | $0 \leq w_{1,2}, h_{1,2} \leq \Lambda$ |
| such that : | $0.1\mu\text{m} \leq t \leq 0.5\mu\text{m}$ |

4. Results & Analysis

Forty representative Pareto-optimal solutions are plotted in Fig.4 for the two gratings having nine arbitrary parameters (A) and (B), and for the two gratings comprised of Si_3N_4 (C) and (D). The net transverse radiation pressure force F_x is plotted against the total mass of the sail, m_{sail} . In all cases a trend in the data appears: Higher mass sails provide higher forces. To select the most optimal design for each structure we use the greatest value of the transverse acceleration $a_x = F_x/m_{\text{sail}}$ as the deciding factor (see straight line in Fig.4). The parameters for the Pareto-optimal solution that intersects this line are tabulated in Table 2 for the four different cases.

We find that both the prismatic and metasurface structures having arbitrary refractive indexes are able to produce large values of F_x , as is evident in Fig.4 for Case A and Case B. However, owing to the lower mass of the metasurface structure, its optimal acceleration $a_x = 1080 [\mu\text{m}/\text{s}^2]$ is 48% greater than that of the prism grating. The Si_3N_4 structures, Case C and Case D, depict significantly less values of optimized acceleration. These values may be compared with a conventional aluminized polyimide sail [22] which is roughly $3 [\mu\text{m}]$ thick and achieves a momentum transfer efficiency of roughly 90% of the ideal value of 0.77 : $a_x = 680 [\mu\text{m}/\text{s}^2]$. This comparison suggests that an optimized metasurface sail is a competitive alternative to a conventional reflective sail. However, amongst the many unknown fabrication, packaging, unfurling, and space weathering issues is whether a large robust metasurface grating can be fabricated on a thin ($< 1 [\mu\text{m}]$) substrate [14].

To better understand the spectral force characteristics of the four sails examined in this study, we plot the transverse spectral force distribution $F_{v,x} = F_{v,x}^s + F_{v,x}^p$ in Fig. 5. The blue line represents the FDTD-obtained values corresponding to the Maxwell stress tensor calculations, whereas the circles represent the values corresponding to our FDTD modal analysis. The excellent agreement between these two approaches provides a level of cross-validation of the methods. Fluctuations of the value of $F_{v,x}$ are indicative of pronounced diffractive variations of the transmitted and reflected light at different optical frequencies, as expected for a small period grating [4]. Also plotted in Fig. 5 are theoretical values of force for the ideal limit $\eta_x = 1$ (black line) and the ideal reflective sail $\eta_x = 0.77$ (red line): $F_{x,v} = \eta_x \tilde{I}vA/c$. These results suggest that the diffractive sails explored in this study may equal or exceed the acceleration of a

Table 2. Optimized parameters and cost function values for (A) prism and (B) meta gratings of arbitrary dispersionless materials, and (C) prism and (D) meta gratings for Si_3N_4 , each with period $\Lambda = 1.5[\mu\text{m}]$, $L_y = 1 [\text{m}]$, $L_x = N\Lambda = 1 [\text{m}]$, $A = L_x L_y$.

| Parameters | A | B | C | D |
|--------------------------------|-------|------|-------------------------|-------------------------|
| $h_1 [\mu\text{m}]$ | 0.76 | 1.12 | 1.02 | 0.62 |
| $h_2 [\mu\text{m}]$ | - | 1.26 | - | h_1 |
| $w_1 [\mu\text{m}]$ | - | 0.32 | - | 0.16 |
| $w_2 [\mu\text{m}]$ | - | 0.16 | - | 0.24 |
| $x_1 [\mu\text{m}]$ | - | 0.06 | - | 0.38 |
| $x_2 [\mu\text{m}]$ | - | 0.44 | - | 0.1 |
| Prism Angle | 26.9° | - | 34.2° | - |
| n_1 | 2.43 | 1.55 | Si_3N_4 | Si_3N_4 |
| n_2 | 1.5 | 1.5 | Si_3N_4 | Si_3N_4 |
| $t [\mu\text{m}]$ | 0.1 | 0.1 | 0.1 | 0.11 |
| Force [nN] | 785 | 787 | 722 | 416 |
| mass [$\times 10^{-3}$ kg] | 1.07 | 0.73 | 1.93 | 0.84 |
| $a_x [\mu\text{m}/\text{s}^2]$ | 731 | 1080 | 373 | 494 |

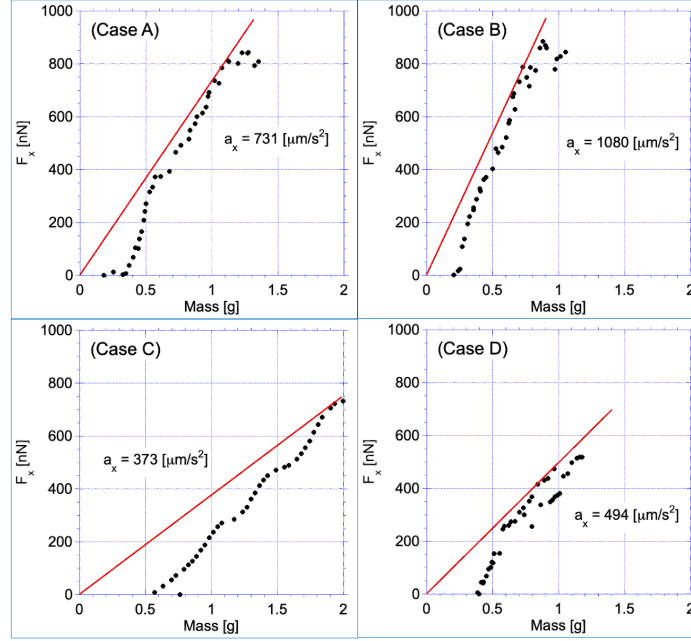


Fig. 4. Pareto optimal solutions for (A) prismatic and (B) metasurface gratings having arbitrary refractive indexes, and for (C) prismatic and (D) metasurface gratings comprise of silicon nitride. A sun-facing square sail of area $1 \text{ [m}^2\text{]}$ illuminated with a band-limited solar black body is assumed. The optimal transverse acceleration a_x for each case is determined from the slope of the straight line, and the corresponding design parameter values for the intersecting points are given in Table 1.

reflective sail only if there is a small-mass advantage of the former. The prism and pillar designs suffer from the effects of external and internal reflections which can scatter light that opposes the desired transverse scattering direction. For example front surface reflections from the prism in Fig. 3 (A) have positive values of k_x which oppose the transmitted (refracted) rays. Those reflected rays carry 17% of incident beam power owing to Fresnel reflections. Less than two thirds of the incident radiation is refracted out the back surface owing to internal reflections and shadowing effects from the steep side facets. It is yet unknown whether the added mass of anti-reflection coatings would provide increased the transverse acceleration. Other unknowns that are beyond the scope of this paper include the practical limits of assumptions about the rigidity of the sail, the coherence properties of the incident sunlight, and whether the sail can be packaged and unfurled without changing its optical properties.

5. Conclusions

We performed FDTD simulations coupled with a NSGA-II multi-objective optimizer to determine design parameters for four different grating structures, each having a period of $1.5 \text{ [}\mu\text{m]}$ and a sail area of $1 \text{ [m}^2\text{]}$. The small grating period was selected to satisfy a small desired mass and a marginal cutoff wavelength of the solar blackbody spectrum. Our optimization study included 3 objectives and up to 9 variables, as well as both s and p polarization. The transverse component of radiation pressure force was determined for a truncated solar black body radiator (200-900 [THz] or equivalently, 0.33 to $1.5 \text{ [}\mu\text{m}]$) at 1 [AU] for the purpose of two-orbit changing maneuvers in space. An optimized metasurface grating comprised of two pillars per period was found to provide 48% more transverse acceleration than an optimized prism grating owing to

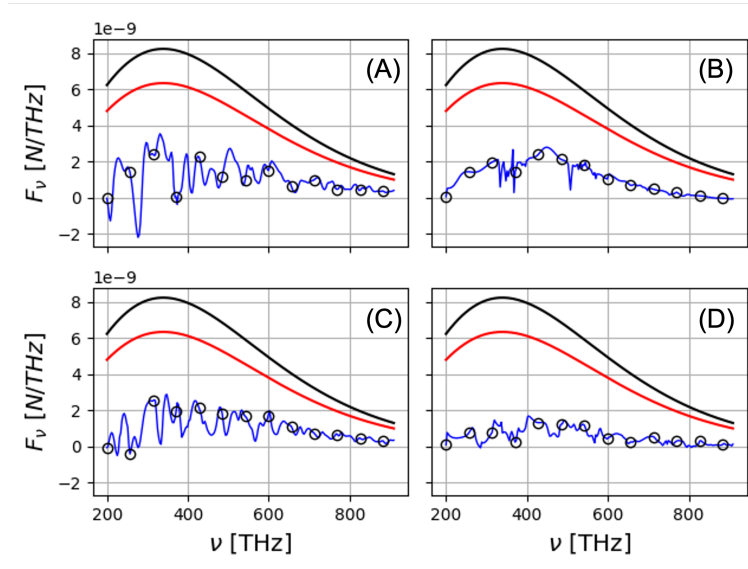


Fig. 5. Spectral transverse force distribution $F_{x,\nu}$ determined from Maxwell stress tensor (blue line) and modal analysis (open circles) for the four cases described in the text, and for an idealized reflective sail (red line) and the upper theoretical bound (black line). An area of 1 m^2 is assumed.

the small mass of the former grating. We found that Silicon Nitride did not perform well for either the prism or two-pillar metasurface design. Although none of the structures provided radiation pressure force values exceeding those of an ideal flat reflective sail, the diffractive sail may nevertheless provide an acceleration advantage if the proposed sun-facing diffractive sail spacecraft has a total lower mass than a reflective sailcraft. The design of alternatives to flat reflective sails is an emerging area of research and we therefore believe continued exploration of diffractive designs such as hybrid reflective/transmissive structures will provide more efficient solar sails in the future.

Funding. National Aeronautics and Space Administration(NASA) (80NSSC19K0975, 80MSFC22F0165), Johns Hopkins University Applied Physics Lab (177864).

Acknowledgment. We are grateful to Charles (Les) Johnson and Andrew F. Heaton (NASA George C. Marshall Space Flight Center, Huntsville, AL), and to Amber L. Dubill (Johns Hopkins Applied Physics Laboratory) for discussions related to solar sailing. We also thank Rajesh Menon and Apratim Majumder (U. Utah, Salt Lake City, UT) for meta-material and FDTD modeling discussions.

Disclosures. The authors declare no conflicts of interest.

Data availability. Data underlying the results presented in this paper are not publicly available at this time but may be obtained from the authors upon reasonable request.

References

1. K. Tsander, "From a scientific heritage, nasa technical translation ttf-541, 1967, a translation of iz nauchnogo naslediya," (1924).
2. K. E. Tsiolkovsky, "Extension of man into outer space," in *Proceedings of the Symposium on Jet Propulsion*, vol. 2 (1921).
3. L. Johnson, G. A. Swartzlander, and A. Artusio-Glimpse, "An overview of solar sail propulsion within nasa," *Adv. Sol. Sail.* pp. 15–23 (2014).
4. G. A. Swartzlander, "Radiation pressure on a diffractive sailcraft," *J. Opt. Soc. Am. B* **34**, C25 (2017).

5. Y.-J. L. Chu, E. M. Jansson, and G. A. Swartzlander, "Measurements of radiation pressure owing to the grating momentum," *Phys. Rev. Lett.* **121**, 063903 (2018).
6. Y.-J. L. Chu, N. V. Tabiryan, and G. A. Swartzlander, "Experimental verification of a bigrating beam rider," *Phys. Rev. Lett.* **123**, 244302 (2019).
7. P. R. Srivastava, Y.-J. L. Chu, and G. A. Swartzlander, "Stable diffractive beam rider," *Opt. Lett.* **44**, 3082 (2019).
8. P. R. Srivastava and G. A. Swartzlander, "Optomechanics of a stable diffractive axicon light sail," *The Eur. Phys. J. Plus* **135** (2020).
9. Y.-J. L. Chu, M. Meem, P. R. Srivastava, R. Menon, and G. A. Swartzlander, "Parametric control of a diffractive axicon beam rider," *Opt. Lett.* **46**, 5141 (2021).
10. S. Firuzi, Y. Song, and S. Gong, "Gradient-index solar sail and its optimal orbital control," *Aerosp. Sci. Technol.* **119**, 107103 (2021).
11. Y. Chu, S. Firuzi, and S. Gong, "Controllable liquid crystal diffractive sail and its potential applications," *Acta Astronaut.* **182**, 37–45 (2021).
12. G. A. Swartzlander, "Theory of radiation pressure on a diffractive solar sail," *J. Opt. Soc. Am. B* **39**, 2556 (2022).
13. A. S. Swakshar, S. M. Kim, and G. A. Swartzlander, "Broadband radiation pressure on a small period diffractive film," *Opt. Express* **30**, 45279 (2022).
14. M. I. Abdelrahman and F. Monticone, "How thin and efficient can a metasurface reflector be? universal bounds on reflection for any direction and polarization," (2022).
15. P. Zhang, S. Firuzi, C. Yuan, X. Gong, and S. Gong, "General passive stability criteria for a sun-pointing attitude using the metasurface sail," *Aerosp. Sci. Technol.* **122**, 107380 (2022).
16. O. Borgue and A. M. Hein, "Transparent occulter: A nearly zero-radiation pressure sunshade to support climate change mitigation," *Acta Astronaut.* **203**, 308–318 (2023).
17. A. F. Oskooi, D. Roundy, M. Ibanescu, P. Bermel, J. Joannopoulos, and S. G. Johnson, "Meep: A flexible free-software package for electromagnetic simulations by the FDTD method," *Comput. Phys. Commun.* **181**, 687–702 (2010).
18. K. Deb, A. Pratap, S. Agarwal, and T. Meyarivan, "A fast and elitist multiobjective genetic algorithm: Nsga-ii," *IEEE transactions on evolutionary computation* **6**, 182–197 (2002).
19. K. Luke, Y. Okawachi, M. R. E. Lamont, A. L. Gaeta, and M. Lipson, "Broadband mid-infrared frequency comb generation in a si_3n_4 microresonator," *Opt. Lett.* **40**, 4823 (2015).
20. NeXolve LaRC CP1 Polyimide, https://www.matweb.com/search/datasheet_print.aspx?matguid=290379e273ae48139ac2628a3a9610e4. Accessed: Jan 2023.
21. W. M. Haynes, D. R. Lide, and T. J. Bruno, *CRC handbook of chemistry and physics* (CRC press, 2016).
22. C. R. McInnes, *Solar Sailing* (Springer London, 1999).